SIRT1 inhibitor EX-527 inhibits ventricular arrhythmias by selectively reducing late Na^+ current in mice ventricular myocytes

Guolan Ma, Zhijie Liu, Min Zhang, Antao Luo*

Institute of Cardiovascular Diseases, Hubei Province Key Laboratory of Occupational Hazard Identification and Control, School of Medicine, Wuhan University of Science and Technology, Wuhan 430065, China

Abstract: A significant aspect in causing arrhythmia in some pathological situations (e.g., myocardial ischemia, heart failure, etc.) is an increase in late sodium current (I_{NaL}) in ventricular myocytes; reduction of I_{NaL} is a novel target for heart failure therapy. Deacetylase SIRT1 has a variety of cardioprotective effects, but whether it exerts antiarrhythmic effects by inhibiting I_{NaL} remains to be studied. In previous experiments, it was found that SRT2104, a specific agonist of SIRT1, could inhibit I_{NaL} and ventricular arrhythmias induced by anemone toxin (ATX II). Furthermore, EX-527, a specific inhibitor of SIRT1, was used for the verification experiment, and it was found that EX-527 could also inhibit I_{NaL}, but there was no study of I_{NaL} by EX-527. In this study, whole-cell patch clamp technique and in vivo electrocardiogram recording were used to investigate the effect and mechanism of EX-527 (10 μM) on I_{NaL} in pathologically enlarged mouse ventricular myocytes such as ATX II (2 nM) or heart failure. The following are the study's main findings: (1) EX-527 inhibited the ATX II-enhanced I_{NaL} (Fig. 1 A, B); (2) The inhibition of ATX II-enhanced I_{NaL} by EX-527 is stronger than that by SRT2104(Fig. 1 C, E); (3) A combined inhibition of CaMKII and PKC nearly completely eliminated the effect of EX-527 to inhibit ATX II-enhanced I_{NaL} (Fig. 2); (4) EX-527 inhibited the TAC-enhanced I_{NaL} (Fig. 3); (5) EX-527 ended the protracted APD and got rid of all EADs brought on by ATX II (Fig. 4); (6) EX-527 dramatically decreased the frequency and length of ATX II-induced VT and VF (Fig. 5).

1. Introduction

An essential ion current in cardiomyocytes is the late Na^+ current (I_{NaL}). Prior research has shown that a number of clinical situations, including heart failure, oxidative stress, hypoxia, and exposure to Na^+-channel toxins like anemone toxin II (ATX II), are associated with elevated levels of I_{NaL}. Elevated intracellular Na^+ and Ca^{2+} overload in cardiomyocytes caused by a substantial increase in Na^+ inflow is linked to elevated diastolic tension and cardiac arrhythmias [1–5]. I_{NaL} inhibitors such as mexiletine and ranolazine reverse the detrimental effects of I_{NaL} enhancers and effectively reduce ventricular arrhythmias induced by ischemia and hypoxia [6]. A previous study in our laboratory also showed that inhibiting endogenous I_{NaL} abolishes ventricular arrhythmias induced by E-4031 and d-sotalol [7]. Thus, the inhibition of I_{NaL} is considered a promising antiarrhythmic strategy.

SIRT1 is a protein deacetylase that is reliant on nicotinamide adenine diphosphate (NAD^+) and has evolved to deacetylate cofactors and transcription factors that control a variety of key metabolic processes [8]. A growing body of research links SIRT1 to defense against cardiovascular conditions such as hypertension, myocardial infarction, and ischemia–reperfusion damage. In rat neonatal cardiomyocytes, the NAD^+ precursor nicotinamide riboside (NR) reduced I_{NaL}, according to Matasic et al. [9]. Previous research in our laboratory also revealed that resveratrol (a SIRT1 activator) inhibited the H_2O_2-induced increase in I_{NaL} in rabbit ventricular myocytes [10]. These reports and our present study show that SIRT1 activation can inhibit ventricular arrhythmias by reducing I_{NaL} in cardiomyocytes. Our previous research demonstrated that SRT2104 (selective SIRT1 activator) can inhibit the ATX II-induced I_{NaL} and reduce the incidence and duration of ATX II-induced ventricular arrhythmias significantly.

Several clinical trials have evaluated the safety, tolerability, pharmacokinetics, and bioavailability of SRT2104. SRT2104 was found to be safe and well tolerated in phase I clinical trials. SRT2104 has shown beneficial effects in cardiovascular diseases; however, no research has yet investigated its effects on I_{NaL} and cardiac arrhythmias. This study used EX-527, a specific SIRT1 inhibitor, to determine whether SRT2104 inhibits I_{NaL} through SIRT1. Surprisingly, the results indicated that EX-527 also inhibits the increase in I_{NaL} induced by ATX II. Although EX-527 has long been used as a tool drug in previous studies, there has been no direct research on its effect on I_{NaL}. These findings contradict the initial hypothesis that EX-527 would increase I_{NaL} by inhibiting

*Corresponding author's email: lat78@126.com

SIRT1. It is speculated that EX-527 may inhibit I_{NaL} through other mechanisms, which remain unclear and warrant further investigation.

2. Materials And Methods

2.1. Solutions

Table 1. displays the solutions used in this investigation.

Table 1. Solutions used in this investigation.

Types of solutions		Reagents (in mM)	pH
Tyrode		0.33 NaH_2PO_4, 1.8 $CaCl_2$, 5.4 KCl, 135 NaCl, 1 $MgCl_2$, 10 glucose, 10 HEPES	7.4
KB		20 taurine, 20 KH_2PO_4, 70 KOH, 40 KCl, 1 Mg Cl_2, 50 L-glutamic acid, 0.5 EGTA, 10 glucose, 10 HEPES	7.4
I_{NaL}	Bath	5.4 CsCl, 1.8 $CaCl_2$, 135 NaCl, 1 $MgCl_2$, 0.33 NaH_2PO_4, 10 glucose, 10 HEPES, 0.3 $BaCl_2$, 0.3 $CdCl_2$	7.4
	Pipette	3 NaCl, 133 CsCl, 2 Na_2ATP, 2 $MgCl_2$, 2 TEACl, 5 HEPES, 10 EGTA	7.3
AP	Bath	0.33 NaH_2PO_4, 135 NaCl, 1.8 $CaCl_2$, 5.4 KCl, 1 $MgCl_2$, 10 glucose, 10 HEPES	7.4
	Pipette	30 KCl, 5 MgATP, 110 K-aspartate, 5 NaCl, 5 creatine phosphate, 0.1 GTP, 10 HEPES, 0.1 EGTA	7.3

2.2. Transverse aortic constriction (TAC) in the mouse

An intraperitoneal dose of 50 mg/kg pentobarbital sodium was used to anesthetize the mice after a week of adaptive feeding. Under a microscope, the mice's second rib was exposed during the thoracotomy procedure. A tiny 6-0 suture was inserted between the innominate artery and the left carotid artery after the placement of the aortic arch was established. The 26 G pads were arranged in an L shape and positioned parallel to the aortic arch, with two loose knots created around the aorta. After fastening, the cushion needle is pulled out quickly to produce the contraction of the diameter 0.4 mm and finally sutured. In the sham operation group, the whole process was the same except for ligating the aorta.

The mouse is given another round of anesthesia one week after TAC in order to assess the extent of pressure overload brought on by transverse aortic ligation. The model was identified by color Doppler flow imaging, and the blood flow velocity at the stenosis of the aortic arch was detected. The peak ratio of blood flow velocity between the successful TAC model and the sham operation group was about 5-10. The successful model mice were continued to feed, and the ventricular structure and cardiac function were measured by M-mode echocardiography at 2, 4, and 8 weeks after the operation.

2.3. Currents and AP recordings

At room temperature (22–25°C), all tests were carried out. With the patch electrodes filled with pipette solution, their resistance ranged from 1.5 to 2.5 MΩ. A two-stage puller (PC-100, Narishige Group, Japan) was used to draw them. Electronic compensation of 60–80% was applied to cell capacitance and series resistances without causing any ringing when used only for voltage-clamp measurements. A 2 kHz filter and 10 kHz digitalization were applied to the currents or APs that were captured using an EPC10 amplifier (HEKA Electronics, Pfalz, Germany). Current density, or pA/pF, was calculated by normalizing current data using the cell capacitance.

Using a 300 ms depolarizing pulse at a frequency of 0.2 Hz, an I_{NaL} was measured between a holding potential (HP) of –90 mV and –20 mV, respectively. To exclude the possibility of I_{NaL} influence, the amplitude of I_{NaL} was calculated using the average current recorded between 190 and 210 ms after the start of the depolarizing pulse. By applying 300-ms depolarization pulses with potentials ranging from –80 mV to +60 mV in 5 mV increments from an HP of –90 mV (0.5 Hz), the current-voltage (I-V) relationship of I_{NaL} was recorded.

APs were stimulated using the current clamp mode of the patch-clamp method with pulses lasting 6 ms, 1.5 times the diastolic threshold current, at various stimulation frequencies. The maximal upstroke velocity (V_{max}), AP duration (APD) at 90% repolarization (APD90), AP amplitude (APA), and resting membrane potential (RMP) were all examined.

2.4. Electrocardiogram (ECG) recording

Following a week of maintenance, the mice were divided into four groups at random: (1) control (physiological saline, iv, n = 5); (2) EX-527 （25 μg/kg EX-527, iv, n = 5); (3) ATX II (100 μg/kg ATX II, iv, n = 10); and (4) ATX II + EX-527 (100 μg/kg ATX II + 25 μg/kg EX-527, iv, n = 10). Pentobarbital sodium was used to anesthetize mice (50 mg/kg, intraperitoneal injection). Surface ECGs were constantly acquired using a DataLAB data collection system (BL-420F, Chengdu Techman Software Co., Chengdu, China) in the lead II configuration. After a 10 min baseline recording, different solutions (200–300 μL) were injected into the tail vein of each mouse for 5 min, followed by a further 55-min recording. Measured were the frequency and duration of ventricular fibrillation (VF) and ventricular tachycardia (VT). The VT and VF were determined according to the Lambeth Conventions standard. VT was considered a run of four or more consecutive ventricular premature beats, and VF was considered a low-voltage and unidentifiable QRS complex.

2.5Data Analysis and statistics

The mean ± SD is used to show the data. matched Student's t tests were used to compare the two groups. For multiple comparisons, one-way analysis of variance was used, followed by the Bonferroni correction. Equipped with Origin 2021 (OriginLab, Northampton, MA, USA), statistical analyses were carried out. Every statistical test had two tails. $P < 0.05$ was used as the threshold for statistical significance.

3. Results

3.1. Effects of EX-527 on INaL in left ventricular myocytes

Using the whole-cell patch-clamp method, we recorded I_{NaL} in ventricular myocytes for this investigation. Incubating the cells in a basal bath solution resulted in a modest and steady amplitude of I_{NaL} (at –20 mV). At one minute after the membrane was ruptured and whole-cell patch mode was attained, I_{NaL} was –0.22 ± 0.05 pA/pF. Nevertheless, after membrane rupture and 15 min ($n = 15$, $P < 0.01$), I_{NaL} rose to –2.88 ± 0.34 pA/pF when 2 nM ATX II was introduced to the bath solution. When ATX II was present, the amplitude of I_{NaL} was considerably reduced by EX-527 (10 µM) to -2.53 ± 0.23 pA/pF ($n = 5$, $P < 0.01$ vs. ATX II; Fig. 1, *A–B*).

In an additional cohort, 45 min later, 45 µM EX-527 significantly reduced I_{NaL} when 2 nM ATX II and 4 µM SRT2104 were present (–1.84 ± 0.23 vs –2.44 ± 0.40 pA/pF, $n = 5$, $P < 0.01$, Fig. 1, *E–F*). In the presence of 2 nM ATX II and 10 µM EX-527, 4 µM SRT2104, however, did not significantly further reduce I_{NaL} (–2.53 ± 0.24 vs. -2.53 ± 0.22 pA/pF, $n = 5$, $P > 0.05$, Fig. 1, *C–D*) at 45 min.

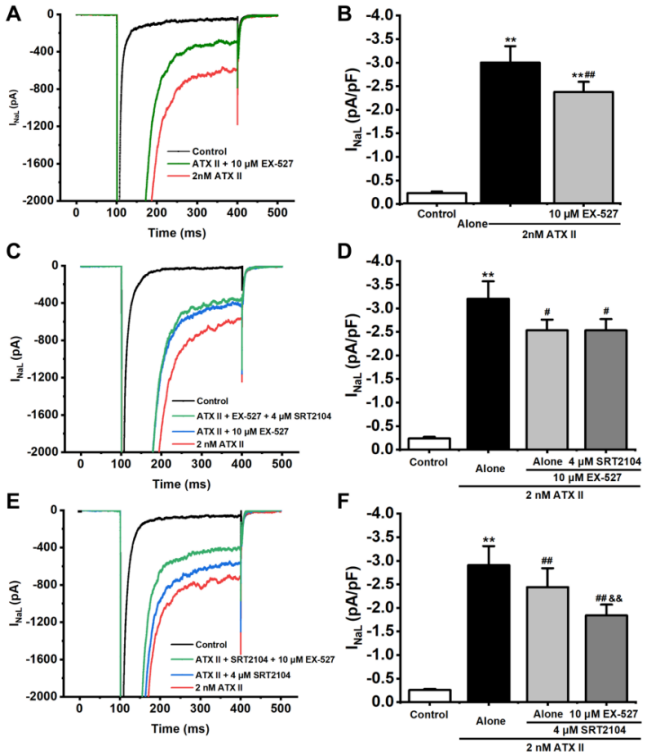

Fig. 1. The enhanced late Na^+ current (I_{NaL}) brought on by anemone toxin II (ATX II) was suppressed by EX-527. Sample whole-cell recordings of INaL in mouse left ventricular myocytes before and after treatment with 10 µM ATX II, in the absence (Control) and in the presence of 2 nM ATX II XX-527 (A, B). Recordings of I_{NaL} representative of two cells consecutively treated to two milligrams of ATX II, ATX II plus four micrograms of SRT2104, and ATX II plus SRT2104 plus ten micrograms of EX-527 (C, D). ATX II, 10 µM EX-527 plus ATX II, and ATX II plus EX-527 plus 4 µM SRT2104 (E, F). Mean ± SD, all n = 5. $^{*}P < 0.05$, $^{**}P < 0.01$ vs control; $^{\#}P < 0.05$, $^{\#\#}P < 0.01$ vs ATX II; $^{\&\&}P < 0.01$ vs ATX II plus SRT2104.

3.2. CaMKII and PKC mediate the inhibitory effect of EX-527 on ATX II-enhanced INaL

After 15 min after membrane rupture, the current density of I_{NaL} increased from a baseline of –0.23 ± 0.03 pA/pF to -2.17–8.17 pA/pF due to the addition of 2 nM ATX II to the bath solution (n = 15, $P < 0.01$). The I_{NaL} was further lowered by the CaMKII inhibitor KN-93 (10 µM) and the PKC inhibitor BIM (2 µM) in the presence of 2 nM ATX II. The decreases occurred at 30 min (n = 5, $P < 0.01$) and were 2.46 ± 0.40 to –1.10 ± 0.23 and 1.67± 0.04 to –0.68 ± 0.15 pA/pF, respectively (Fig. 2, *A-D*). Additionally, after 45 min, 10 µM EX-527 further reduced I_{NaL} in the presence of 2 nM ATX II and 10 µM KN-93/2 µM BIM (–0.59 ± 0.14 vs. –1.10 ± 0.23 pA/pF or –0.47 ± 0.09 vs. –0.68 ± 0.15 pA/pF, n = 5, $P < 0.01$).

By contrast, when 2 nM ATX II was present for 30 min, the combination of KN-93 (10 µM) and BIM (2 µM) reduced I_{NaL} from –2.38 ± 0.29 to –1.24 ± 0.12 pA/pF (n = 5, $P < 0.01$). In the presence of 2 nM ATX II and KN-93 + BIM, 10 µM EX-527, however, did not significantly further reduce I_{NaL} (–1.21 ± 0.11 pA/pF, n = 5, $P > 0.05$ vs. KN-93 + BIM) at 45 min (Fig. 2, *E–F*). The ability of

EX-527 to inhibit ATX II-enhanced I_{NaL} was almost entirely decreased by the combined inhibition of PKC and CaMKII, indicating that CaMKII and PKC mediate the inhibitory impact of EX-527 on ATX II-enhanced I_{NaL}.

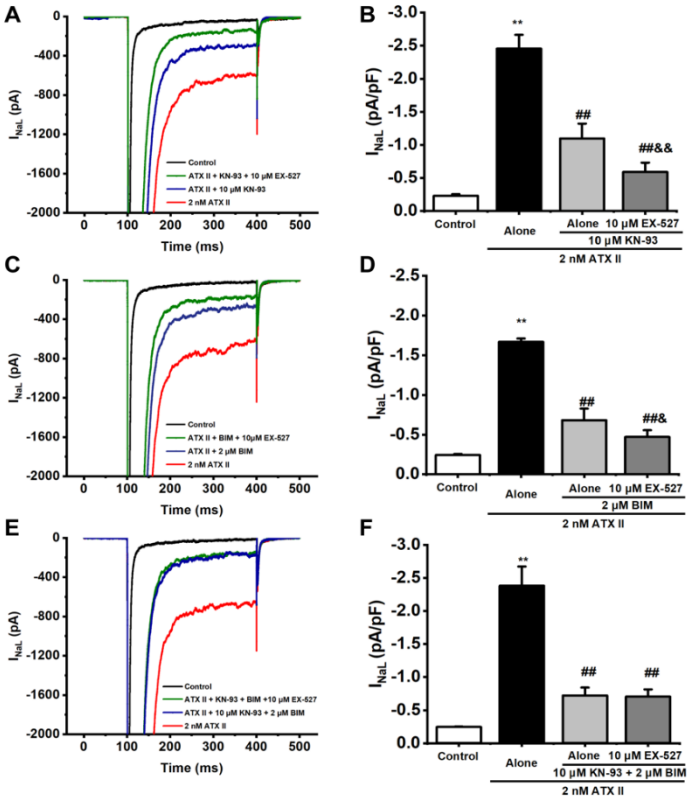

Fig. 2. Impact of EX-527 on ATX II-stimulated INaL both alone and in combination with PKC inhibitor (BIM) and CaMKII (KN-93). In three cells that were treated to 2 nM ATX II, 10 μM KN-93, and 4 μM SRT 2044, respectively, representative recordings of I_{NaL} were made (A), ATX II, ATX II plus 2 μM BIM, and ATX II plus BIM plus SRT 2104 (C), or ATX II, ATX II plus KN-93 plus BIM, and ATX II plus KN-93 plus BIM plus SRT 2104 (E). Data summary for the average current density of I_{NaL} for all conducted tests, as shown in A (B), C (D), and E (F). Mean ± SD, all n = 5. $^{**}P < 0.01$ vs control; $^{\#\#}P < 0.01$ vs ATX II; $^{\&}P < 0.05^{\&\&}$, $P < 0.01$ either vs ATX II plus 10 μM KN-93 (B) or ATX II plus 2 μM BIM (D).

3.3. Effects of EX-527 on INaL in left ventricular myocytes of mice with TAC

It is anticipated that mice given TAC will have heart dilatation after 6–8 weeks and hypertrophy within 1-2 weeks. Ventricular myocytes extracted from mice administered TAC for 8 weeks showed an increase in cell capacitance of 412.75 ± 79 pF (n = 6, $P < 0.01$ vs. 204.79 ± 46 pF) and an increase in I_{NaL} to 0.49 ± 0.04 pA/pF (n = 6). When 10 μM EX-527 was added to the bath solution, 15 min after membrane rupture, the current density of I_{NaL} was inhibited to –0.28 ± 0.05 pA/pF (n = 15, $P < 0.01$ vs. TAC). 36.5 ± 7.9% (n = 5) is the inhibition rate (Fig. 3, *A*–*D*).

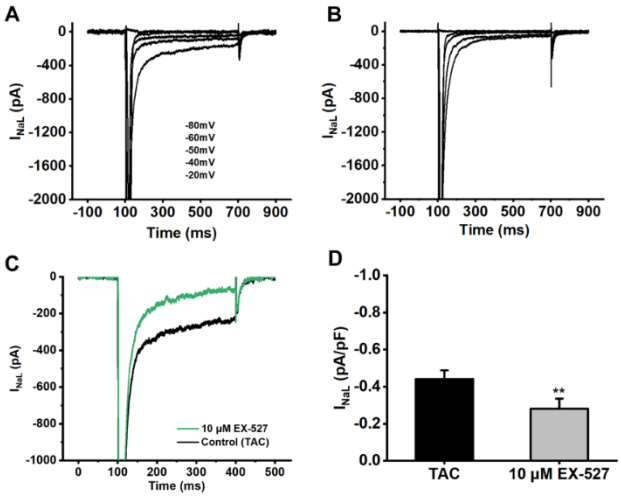

Fig. 3. Effects of EX-527 on TAC-stimulated I_{NaL}. The current-voltage (I-V) relationship for I_{NaL} in TAC mice left ventricular myocytes before and after treatment with 10 μM EX-527 (A, B). Representative whole-cell recordings of I_{NaL} in TAC mice left ventricular myocytes before and after treatment with 10 μM EX-527 (C, D). Mean ± SD, n = 5. $^{**}P < 0.01$ vs TAC.

3.4. Effects of EX-527 on ATX-induced EADs

APs in left ventricular myocytes were captured utilizing the patch-clamp technique's current clamp mode. EX-527 (10 μM) did not significantly affect AP when there was no medication present (Table 2).

ATX II (2 nM) markedly prolonged APD_{90} in ventricular myocytes from 35 ± 2 to 2156 ± 58 ms (n = 10, P < 0.01 vs. control) and induced early afterdepolarizations (EADs) in 10/10 cells. In the presence of ATX II, 10 μM EX-527 significantly shortened the prolonged APD_{90} to 97 ± 15 ms (n = 10, P < 0.01 vs. ATX II) and completely eliminated EADs (0/10 cells). Remarkably, the APD_{90} was extended to 2078 ± 31 ms after the EX-527's washing in a bath solution containing 2 nM ATX II (n = 10, P < 0.01 vs. ATX II + EX-527), and EADs reoccurred in 10/10 cells (Fig. 4), demonstrating that the effects of EX-527 on ATX II-induced AP changes were reversible.

Table 2. Impact of EX-527 (10 μM) on mouse left ventricular myocyte action potentials in a control setting.

Parameter	Control	10 μM EX-527	Wash out
RMP (mV)	-74 ± 3	-74 ± 2	-72 ± 3
APA (mV)	130.6 ± 5.5	130.1 ± 1.3	129.8 ± 3.7
APD_{90} (ms)	34 ± 2	34 ± 4	24 ± 3
V_{max} (V/s)	345 ± 57	340 ± 35	348 ± 15

Means ± SD (n = 5–7, stimulation frequency = 1 Hz). RMP, resting membrane potential; APD_{90}, action potential duration at 90% repolarization; APA, action potential amplitude; V_{max}, maximum upstroke velocity. Differences between groups were assessed with one-way ANOVA.

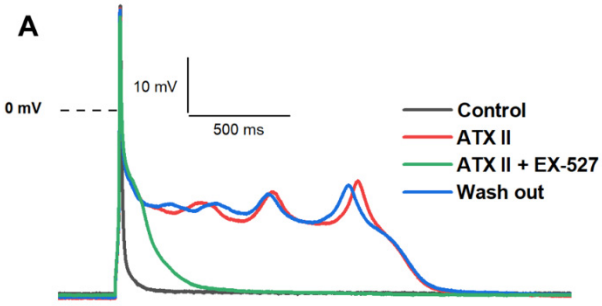

Fig. 4. Impact of EX-527 on AP alterations in mouse left ventricular myocytes caused by ATX II. Representative AP recordings in a ventricular myocyte sequentially exposed to 2 nM ATX II, ATX II plus 10 μM EX-527, and washing with ATX II.

3.5. Effects Of Ex-527 On Atx Ii-Induced Ventricular Arrhythmia in Mice

In this study, surface ECGs were recorded in anesthetized mice before and after tail vein injection of different solutions. EX-527 (25 μg/kg) had no significant effect on ECGs (Fig. 5, *A*). 100 μg/kg ATX II induced VT and VF in 100% (10/10) and 90% (9/10) of the animals, respectively, and the durations of VT and VF were 2180 and 1791 s (VT and VF occurred intermittently, and the duration was the total for each period), respectively (Fig. 5, *B, D-E*). The incidence of VT and VF substantially lowered to 40% (4/10) and 10% (1/10) in rats treated with 100 μg/kg ATX II + 25 μg/kg EX-527. Moreover, the lengths of VF and VT dropped to 27 and 404 s, respectively (Fig. 5, *C–E*). EX-527 dramatically decreased the frequency and length of ATX II-induced VT and VF.

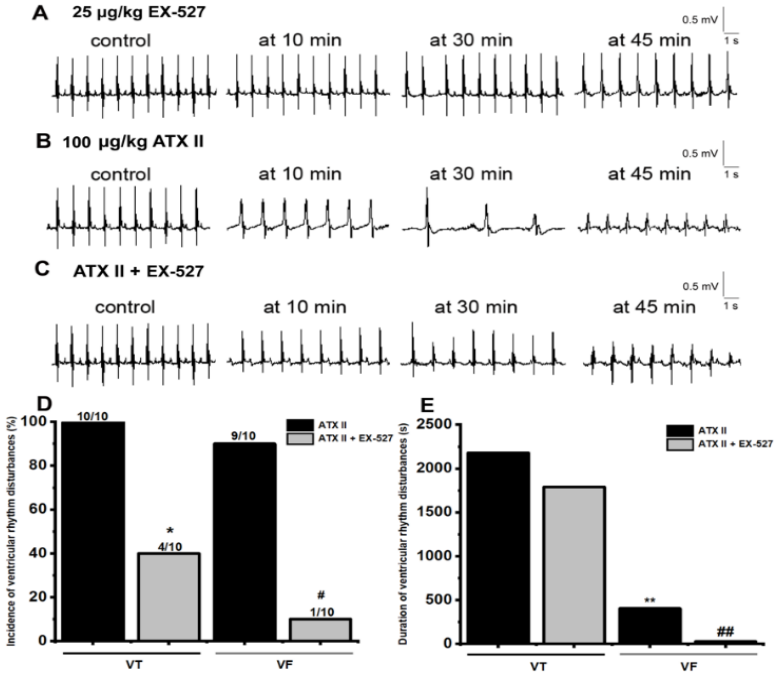

Fig. 5. EX-527 inhibited ATX II-induced ventricular arrhythmias. Representative surface electrocardiogram (ECG) recordings in 3 anesthetized mice before and at 10, 30, and 45 min after exposure to 25 μg/kg EX-527 (A), 100 μg/kg ATX II (B), or ATX II plus EX-527 (C). Ventricular tachycardia (VT) and ventricular fibrillation (VF) incidence and duration (D and E, respectively) in the ATX II and ATX II plus EX-527 groups are summarized. Mean ± SD, n = 10. $^{*}P < 0.05$, $^{**}P < 0.01$ ATX II vs ATX II plus EX-527; $^{\#}P < 0.05$, $^{\#\#}P < 0.01$ ATX II vs ATX II plus EX-527.

4. Discussion

We examined the mechanism behind the effects of the SIRT1 inhibitor EX-527 on I_{NaL} in the ventricular myocytes of mice treated with TAC in this work. The major findings in this study were that (1) EX-527 inhibited the ATX II-enhanced I_{NaL} (Fig. 1, *A-B*); (2) The inhibition of ATX II-enhanced I_{NaL} by EX-527 is stronger than that by SRT2104(Fig. 1, *C-E*); (3) A combined inhibition of CaMKII and PKC nearly completely eliminated the effect of EX-527 to inhibit ATX II-enhanced I_{NaL} (Fig. 2); (4) EX-527 inhibited the TAC-enhanced I_{NaL} (Fig. 3); (5) EX-527 ended the protracted APD and got rid of all EADs brought on by ATX II (Fig. 4); (6) EX-527 dramatically decreased the frequency and length of ATX II-induced VT and VF (Fig. 5).

Extensive research indicates that the inhibition of I_{NaL} effectively reduces ventricular arrhythmias. Ranolazine (I_{NaL} specific inhibitor) can prevent arrhythmias by blocking I_{NaL} [11]; resveratrol (a SIRT1 activator) inhibited the H_2O_2-induced increase in I_{NaL} in rabbit ventricular myocytes [10]. A growing body of research links SIRT1 to defense against cardiovascular conditions such as hypertension, myocardial infarction, and ischemia–reperfusion damage. However, there is little research on the antiarrhythmic properties of SIRT1 and its effects on I_{NaL}. Even there are conflicting results in research on the effects of SIRT1 on I_{NaL}. Vikram et al. [12] reported that there were no changes in I_{NaL} in cSIRT1$^{-/-}$ cardiomyocytes or SIRT1-overexpressing HEK293 cells. However, Yang et al. [13] showed that I_{NaL} was greater in cSIRT1$^{-/-}$ myocytes than in control myocytes. To reduce INaL in rat neonatal cardiomyocytes, Matasic et al. [9] found nicotinamide riboside (NR), a NAD^+ precursor. Furthermore, our previous research found that the SIRT1-specific activator SRT2104 can inhibit the ATX II-induced and TAC-induced INaL (Fig. 1, A, Fig. 3). These results suggest that SIRT1 activation may exert an antiarrhythmic effect by inhibiting I_{NaL}. This study used EX-527, a specific SIRT1 inhibitor, to determine whether SRT2104 inhibits I_{NaL} through SIRT1. Surprisingly, the results indicated that EX-527 also inhibits the increase in I_{NaL} induced by ATX II. Although EX-527 has long been used as a tool drug in previous studies, there has been no direct research on its effect on I_{NaL}. These findings contradict the initial hypothesis that EX-527 would increase I_{NaL} by inhibiting SIRT1. It is speculated that EX-527 may inhibit I_{NaL} through other mechanisms, which remain unclear and warrant further investigation.

Our earlier studies showed that CaMKII and PKC both mediate the impact of elevated intracellular Ca^{2+} on increasing I_{NaL} in ventricular myocytes [14]. In the current investigation, ATX II-enhanced I_{NaL} was decreased by the CaMKII inhibitor KN-93 and the PKC inhibitor BIM by 61.0% and 69.2%, respectively, and I_{NaL} was further inhibited by EX-527 by 22.7% and 14.8%, respectively (Fig. 3, *A-B*). Moreover, the potential of EX-527 to enhance I_{NaL} was totally counteracted by the combination of KN-93 and BIM. These results demonstrate that EX-527 inhibits ATX II-stimulated I_{NaL} via CaMKII and PKC. Moreover, extensive evidence indicates that CaMKII and PKC are important signaling molecules implicated in the development of cardiac arrhythmias. Prior research has shown that elevated CaMKII activity stimulates Ca^{2+} leakage from the sarcoplasmic reticulum (SR) via the ryanodine receptor (SR). Ca^{2+} release pathways and arrhythmias of the ventricle [15]. Moreover, ATX II-induced proarrhythmic changes can be significantly attenuated by CaMKII inhibition [16]. An increase in I_{NaL} leads to intracellular Na^+ overload, which can cause intracellular Ca^{2+} overload via the sarcolemmal Na^+-Ca^{2+} exchanger. Both intracellular Ca^{2+} overload and oxidative stress activate CaMKII, which subsequently phosphorylates cardiac Na^+ channels and ryanodine receptors and further increases I_{NaL} and Ca^{2+} release from the SR [17]. Thus, a vicious cycle of increased I_{NaL} and intracellular Ca^{2+} overload occurs in cardiomyocytes. In this study, EX-527 disrupted the cell cycle by reducing I_{NaL}, thus inhibiting ventricular arrhythmias.

Patients with heart failure have a 50% chance of sudden mortality, a 40% chance of atrial fibrillation, and a 90% chance of ventricular arrhythmia. Sudden cardiac death is mostly caused by these arrhythmias. The prominent arrhythmogenic effect of heart failure is caused by its electrical remodeling. As heart failure progresses, alongside anatomical and morphological changes in the heart, there is damage to cardiac electrical function. Early adaptive changes in electrical function occur simultaneously, playing a compensatory role in maintaining the impaired cardiac function. For instance, in heart failure, the enlargement of cardiomyocytes can increase sodium-calcium exchange (NCX), thereby enhancing myocardial contractility. This adaptive change in the heart's electrical function is referred to as the electrical remodeling of heart failure. Eventually, these compensatory electrical remodeling causes I_{NaL} calcium overload and early and late afterdepolarizations, leading to various arrhythmias. In pathological situations such as cardiomyopathy, heart failure, and ischemia, an increase in I_{NaL} will lengthen the APD, increase the transmural dispersion of repolarization, and result in cardiac arrhythmias. Ventricular arrhythmias under prolonged QT circumstances are believed to be produced by EAD-induced triggering activity [18]. In this investigation, 100% of ventricular myocytes had EADs, and APD90 was markedly extended by ATX II. By lowering I_{NaL}, EX-527 reduced the extended APD90 and removed EADs brought on by ATX II (Fig. 4). EX-527 was shown to be efficient in reducing the occurrence and duration of ventricular arrhythmias, such as VT and VF, that are generated by ATX II, based on the ECG data (Fig. 5). Our results demonstrated that EX-527 inhibited ventricular arrhythmias by reducing I_{NaL}, which was consistent with previous reports that SIRT1 activation by resveratrol and NAD^+ suppresses ventricular arrhythmias. Furthermore, this study also found that EX-527 can inhibit the increased I_{NaL} induced by heart failure (caused by TAC). It is further speculated that EX-527 may have an anti-arrhythmic effect in heart failure, which needs further study.

When it comes to diseases like heart failure, the increase in I_{NaL} is a crucial cause of arrhythmia. Early SGLT2 inhibitors, such as dapagliflozin and

empagliflozin, can improve cardiac function, reduce mortality in heart failure, and selectively inhibit H_2O_2-induced increases in I_{NaL} [19]. Ranolazine, a specific I_{NaL} inhibitor, aids in the treatment of elevated end-diastolic pressure in the left ventricle and malfunction in the right ventricle during heart failure [20], and can effectively improve cardiac function in mice [21]. Therefore, inhibiting I_{NaL} is of great significance in treating heart failure. Our study showed that the I_{NaL} of ventricular myocytes in acutely isolated TAC mice was abnormally large, and EX-527 (10 μM) significantly inhibited this abnormal enlargement of I_{NaL} in TAC mice. This suggests that EX-527 can benefit the heart by reducing arrhythmia occurrence through inhibiting heart failure-induced enlarged I_{NaL}.

In conclusion, our results showed that EX-527 inhibited ventricular arrhythmias by reducing I_{NaL}. However, EX-527 has primarily been used as a tool drug in previous studies of heart failure. For example, co-adding EX-527 (10 μM) can reduce the protective effect of NaSH on heart failure-induced apoptosis [22], co-adding EX-527 can increase acetyl-p53 levels, decrease the NAD/NADH ratio, and eliminate the cardioprotective effect of taurine on TAC mice [23], as well as increase oxidative stress and apoptosis. In these studies, EX-527 showed adverse effects on heart failure, deviating from our experimental results, suggesting that EX-527 may inhibit I_{NaL} through other mechanisms. We speculate that this difference may arise because previous studies added EX-527 together with a target drug, whereas this study added EX-527 alone to examine its direct effect on I_{NaL}. According to our results, EX-527 can exert an antiarrhythmic effect by inhibiting I_{NaL} and also has an inhibitory effect on heart failure-induced I_{NaL}. It can be further speculated that EX-527 has a potential anti-heart failure effect, which warrants further investigation. Additionally, it is necessary to further verify and analyze the previously reported adverse effects of EX-527 on cardiac protection.

References

1. Plant LD, Xiong D, Romero J, Dai H, Goldstein SAN, Hypoxia produces pro-arrhythmic late sodium current in cardiac myocytes by sumoylation of NaV1.5 channels, Cell Rep. 30 (2020) 2225–2236.
2. Zeng B, Liao X, Liu L, Ruan H, Zhang C, Thyroid hormone diminishes Ca2+ overload induced by hypoxia/reoxygenation in cardiomyocytes by inhibiting late sodium current and reverse-Na+/Ca2+ exchange current, Pharmacology. 105 (2020) 63–72.
3. Yu S, Li G, Huang CL, Lei M, Wu L, Late sodium current associated cardiac electrophysiological and mechanical dysfunction, Pflugers Arch. 470 (2018) 461–469.
4. Lin Q, Zuo W, Liu Y, Wu K, Liu Q, NAD+ and cardiovascular diseases, Clin Chim Acta. 515 (2021) 104–110.
5. Shryock JC, Song Y, Rajamani S, Antzelevitch C, Belardinelli L, The arrhythmogenic consequences of increasing late INa in the cardiomyocyte, Cardiovasc Res. 99 (2013) 600–611.
6. Antzelevitch C, Nesterenko V, Shryock JC, Rajamani S, Song Y, Belardinelli L, The role of late INa in development of cardiac arrhythmias, Handb Exp Pharmacol. 221 (2014) 137–168.
7. Serio S, Pagiatakis C, Musolino E, et al. Cardiac aging is promoted by pseudohypoxia increasing p300-induced glycolysis, Circ Res. 133 (2023) 687–703.
8. Chen C, Zhou M, Ge Y, Wang X, SIRT1 and aging related signaling pathways, Mech Ageing Dev. 187 (2020) 111215.
9. Matasic DS, Yoon JY, McLendon JM, et al. Modulation of the cardiac sodium channel NaV1.5 peak and late currents by NAD+ precursors, J Mol Cell Cardiol. 141 (2020) 70–81.
10. Qian C, Ma J, Zhang P, et al. Resveratrol attenuates the Na+-dependent intracellular Ca2+ overload by inhibiting H2O2-induced increase in late sodium current in ventricular myocytes, PLoS one. 7 (2012) e51358.
11. Miranda VM, Beserra SS, Campos DR. Inotropic and Antiarrhythmic Transmural Actions of Ranolazine in a Cellular Model of Type 3 Long QT Syndrome, Arq Bras Cardiol. 114(2020) 732-735.
12. Vikram A, Lewarchik CM, Yoon JY, et al. Sirtuin 1 regulates cardiac electrical activity by deacetylating the cardiac sodium channel, Nat Med. 23 (2017) 361–367.
13. Yang HY, Lin FZ, Yang HW, et al. The effect of Sirt1 deficiency on Ca2+ and Na+ regulation in mouse ventricular myocytes, J Cell Mol Med. 24 (2020) 6762–6772.
14. Ma J, Luo A, Wu L, et al. Calmodulin kinase II and protein kinase C mediate the effect of increased intracellular calcium to augment late sodium current in rabbit ventricular myocytes, Am J Physiol Cell Physiol. 302 (2012) C1141-51.
15. Mohler PJ, Hund TJ, Role of CaMKII in cardiovascular health, disease, and arrhythmia, Heart Rhythm. 8 (2011) 142–144.
16. Liang F, Fan P, Jia J, et al. Inhibitions of late INa and CaMKII act synergistically to prevent ATX-II-induced atrial fibrillation in isolated rat right atria, J Mol Cell Cardiol. 94 (2016) 122–130.
17. Kornyeyev D, El-Bizri N, Hirakawa R, et al. Contribution of the late sodium current to intracellular sodium and calcium overload in rabbit ventricular myocytes treated by anemone toxin. American journal of physiology, Am J Physiol Heart Circ Physiol. 310 (2016) H426–H435.
18. Burashnikov A, Antzelevitch C, Late-phase 3 EAD. A unique mechanism contributing to initiation of atrial fibrillation, Pacing Clin Electrophysiol. 29 (2006) 290–295.

19. Philippaert K, Kalyaanamoorthy S, Fatehi M, et al. Cardiac late sodium channel current is a molecular target for the sodium/glucose cotransporter 2 inhibitor empagliflozin. Circ. 143(2021) 2188-2204.
20. Kourampi I, Katsioupa M, Oikonomou E, et al. The role of ranolazine in heart failure-current concepts. Am J Cardiol. 209(2023) 92-103.
21. Cempaka DKS, Andrianto A, Al-Farabi MJ, et al. Efficacy of ranolazine to improve diastolic performance in heart failure with preserved ejection fraction: a systematic review and meta-analysis. Eur Cardiol. 189(2023) e02.
22. Wu D, Hu Q, Liu X, et al. Hydrogen sulfide protects against apoptosis under oxidative stress through SIRT1 pathway in H9c2 cardiomyocytes. Nitric Oxide. 46(2015) 204-12.
23. Liu J, Ai Y, Niu X, et al. Taurine protects against cardiac dysfunction induced by pressure overload through SIRT1-p53 activation. Chem Biol Interact. 317(2020) 108972.